

## Article

# Reduction of Residual Quenching Stresses in 2A14 Aluminum Alloy Tapered Cylinder Forgings via a Novel Cold Bulging Process

Bingxiang Wang <sup>1,2,3</sup> , Youping Yi <sup>1,2,3,\*</sup>, Shiquan Huang <sup>1,2,3,\*</sup> and Hailin He <sup>1,2,3</sup>

<sup>1</sup> School of Mechanical and Electrical Engineering, Central South University, Changsha 410083, China; wangbingxiang@csu.edu.cn (B.W.); hehailin0621@126.com (H.H.)

<sup>2</sup> State Key Laboratory of High Performance Complex Manufacturing, Changsha 410083, China

<sup>3</sup> Research Institute of Light Alloy, Central South University, Changsha 410083, China

\* Correspondence: yyp@csu.edu.cn (Y.Y.); huangshiquan@csu.edu.cn (S.H.)

**Abstract:** This study combined finite element method (FEM) simulations and physical experiments to develop a novel cold bulging process, with the aim of studying and mitigating the quenching residual stresses in 2A14 tapered cylinder forgings. The samples underwent cold bulging at different ratios (0–4.0%) to evaluate the residual stress reduction performance (via the hole-drilling strain-gauge method) and the improvements in their mechanical properties. The FEM simulation and experimental results revealed that our proposed cold bulging process reduced the quenching residual stresses by up to 85–87%. The density and uniformity of the precipitated phases increased along with the extent of cold bulging, as confirmed by transmission electron microscope (TEM) observations. Furthermore, compared to the unprocessed samples, the tensile and yield strengths, and elongation of the samples with 3% cold bulging were significantly enhanced (65 MPa, 55 MPa, and 1.7%, respectively).

**Keywords:** 2A14 aluminum alloy; tapered cylinder forging; FEM simulation; residual stress reduction; quenching stress; cold bulging



**Citation:** Wang, B.; Yi, Y.; Huang, S.; He, H. Reduction of Residual Quenching Stresses in 2A14 Aluminum Alloy Tapered Cylinder Forgings via a Novel Cold Bulging Process. *Metals* **2021**, *11*, 717. <https://doi.org/10.3390/met11050717>

Academic Editor: Kohichi Sugimoto

Received: 1 April 2021

Accepted: 24 April 2021

Published: 27 April 2021

**Publisher's Note:** MDPI stays neutral with regard to jurisdictional claims in published maps and institutional affiliations.



**Copyright:** © 2021 by the authors. Licensee MDPI, Basel, Switzerland. This article is an open access article distributed under the terms and conditions of the Creative Commons Attribution (CC BY) license (<https://creativecommons.org/licenses/by/4.0/>).

## 1. Introduction

In order to obtain high mechanical properties, precipitation-hardened aluminum alloys must undergo a quenching process, which includes rapid cooling from the solution temperature [1,2]: the faster the cooling rate, the higher the resulting strength. However, quenching is a complex thermomechanical process and when an object undergoes inhomogeneous plastic deformation due to non-uniform temperature distribution, severe quench residual stresses can develop. Generally, the sign (+ or –) of the residual stress is opposite to that of the plastic strain that caused it [3]. For example, if an initial tensile plastic strain is generated at the rapid cooling edge of the material at the beginning of quenching, as the temperature of the block drops, the surface plastic strain decreases with the development of the compression stress, resulting in the generation of compression stress on the surface and residual tensile stress in the center. As such, compressive residual stress may improve the fatigue life and stress corrosion of aluminum alloy components. On the other hand, residual stress may cause cracks and lead to premature failure [4,5], reduce fatigue strength, and induce dimensional alterations during the processing of the alloys. All the above factors can severely compromise the mechanical properties and dimensional stability of aluminum alloy materials. Therefore, predicting the residual stress generation pattern is crucial for effectively reducing it, thereby improving the quality and reliability of aluminum alloy components.

Numerous researchers have extensively studied the residual stress generation mechanism induced by quenching. For example, M Araghchi et al. [6] studied the influence of the quenching conditions on the residual stress and strength of 2024 aluminum alloys. Gür et al. [7] studied the effects of size and geometry on the residual stress distribution.

Cold working [8–10], pulsed magnetic treatment [11,12], pulsed magnetic field and pushed current combined treatment [13], and heat treatment methods [14,15] have been widely employed to regulate the residual stress. Quenching residual stress is a stress system that manifests in a body when it is free from external forces. Therefore, residual stresses can be effectively relieved by plastic deformation through cold working methods (compression and stretching). Compression is a widely employed method for controlling residual stresses in components with simple shapes and parallel surfaces. Similarly, stretching is a highly effective method for reducing residual stresses in rectangular and symmetric parts, as confirmed by production and experimental reports. Particularly, Koç et al. [3] reported that both the compression and stretching processes were capable of reducing the residual stresses of 7050 forged blocks by more than 90%. Yang et al. [9] employed a cold stretching process (1.5% stretching at a speed of 0.5 mm/s), effectively reducing the quenching residual stress of an A357 aluminum alloy cylindrical bar by 81.5–94.9%. More importantly, when cold deformation was applied between the solution treatment and aging steps, the mechanical properties of the resulting aluminum alloys were notably improved. For example, Li [16] and Ghosh [17] found that cold deformation after solid solution is beneficial to reduce the activation energy of secondary precipitation so as to improve mechanical properties of the Al-Cu-Si-Mg alloy. He et al. [18] demonstrated that as the extent of cold deformation increased, the driving force of precipitation during the aging treatment process also increased, and the mechanical properties of the 2219 aluminum alloy were correspondingly enhanced.

Heat-treatable 2xxx high-strength deformed aluminum alloys are widely used in the aerospace industry due to their low weight [19,20]. For example, large 2A14 tapered cylinder forgings are often used to process large thin-walled load-bearing components. The solution and quenching treatments are crucial processes which endow the tapered cylindrical forgings with high mechanical properties; however, they significantly contribute to the generation of quenching residual stress. Owing to the size and asymmetric structure of the tapered cylinder forgings, the reduction in residual stress by applying conventional compression and stretching cold deformation techniques is not feasible. To compensate for the challenging structural characteristics of tapered cylinder forgings, a novel cold bulging process is required to achieve residual stress relief. Compressing along the taper of the cylinder forging to attain uniform plastic deformation could provide a viable approach to the above objective.

In this study, we conducted cold bulging experiments on reduced-scale 2A14 aluminum alloy tapered cylinder forgings, with the aim of developing a cost-effective and suitable cold working method for residual stress reduction. The residual stresses of the samples after the quenching and cold bulging treatments were measured using the hole drilling strain-gauge method. Based on the elasto-plastic model of the material, the quenching and subsequent cold bulging processes of the 2A14 aluminum alloy tapered cylinder forgings were simulated using the finite element method (FEM), in order to predict the evolution pattern of residual stress during the manufacturing process. The results of the FEM simulation were compared with the experimental measurements to verify their accuracy. In addition, tensile strength tests and transmission electron microscopy (TEM) analysis were employed to study the mechanical properties and microstructures of the heat-treated samples and analyze the effects of cold bulging on their mechanical properties in detail.

## 2. Materials and Experimental Procedures

The experimental materials were sawn from a homogenized 2A14 aluminum alloy ingot and their chemical compositions are given in Table 1. Figure 1 illustrates the manufacturing process of the 2A14 taper cylinder forgings. First, four small taper cylinder forgings were manufactured via hot forging, and subsequently machined into a reduced-scale tapered cylinder forging (dimensions shown in Figure 2). Table 2 provides the detailed conditions of the cold bulging experimental process. The samples were subjected to solution heat treatment at  $500 \pm 3$  °C for 4 h, before being immersed and quenched in water at 20 °C.

Next, samples A and B were subjected to natural aging and artificial aging, respectively. Samples C and D were subjected to cold bulging (Figure 3). The cold bulging process was implemented to compress the reduced-scale tapered cylinder forgings using a bulging die with the appropriate taper scale. The cold bulging ratios of samples C and D were 2 and 3%, respectively. Subsequently, the samples were aged at  $160 \pm 3$  °C for 4 h, and the time interval between the quenching and aging stages did not exceed 4 h.

**Table 1.** Chemical compositions of 2A14 aluminum alloy (wt%).

Element	Cu	Mg	Si	Mn	Fe	Zn	Ti	Ni	Al
Nominal	3.8–4.8	0.4–0.8	0.6–1.2	0.4–1.0	<0.7	<0.3	<0.15	<0.1	Bal.
In this study	4.40	0.48	0.98	0.75	0.20	0.03	0.05	0.01	Bal.

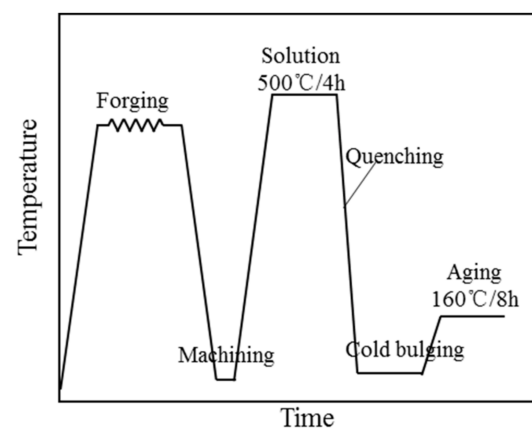


**Figure 1.** Manufacturing process of the 2A14 tapered cylinder forgings.

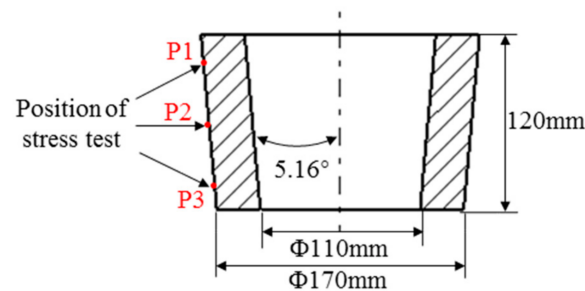


**Figure 2.** Dimensions of the reduced-scale tapered cylinder forging samples and stress test locations.

**Table 2.** Summary of cold bulging treatment conditions.

Sample	Solution Treatment	Quench	Cold Bulging	Aging
A	500 °C for 4 h	Water quenching (<20 °C)	None	Nature aging
B	500 °C for 4 h	Water quenching (<20 °C)	None	Artificial aging (160 °C for 8 h)
C	500 °C for 4 h	Water quenching (<20 °C)	2.0%	Artificial aging (160 °C for 8 h)
D	500 °C for 4 h	Water quenching (<20 °C)	3.0%	Artificial aging (160 °C for 8 h)

The residual stresses of the samples were measured using the hole drilling strain-gauge method, in accordance with the GB/T 31310-2014 standard. As shown in Figure 4, TJ120-1.5-Ø1.5 type A strain-gauge rosettes were attached to the test points following the procedure provided by the Zheng Zhou Research Institute of Mechanical Engineering Co. Ltd., Zhengzhou, China. During the residual stress measurements, 2 mm deep holes

were drilled at the test points using a HK21B type drilling device. For all residual stress measurements, the center of the drill hole and strain rosette were at the same position.

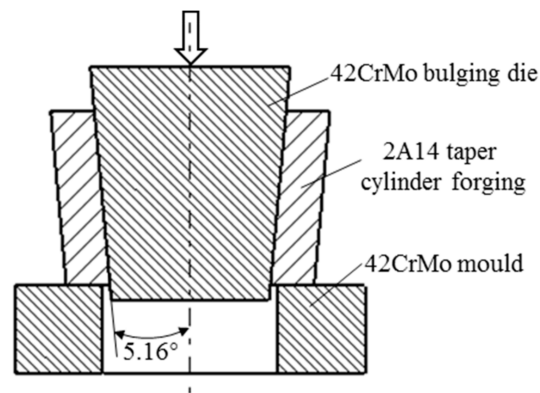


**Figure 3.** Schematic diagram of the cold bulging process.

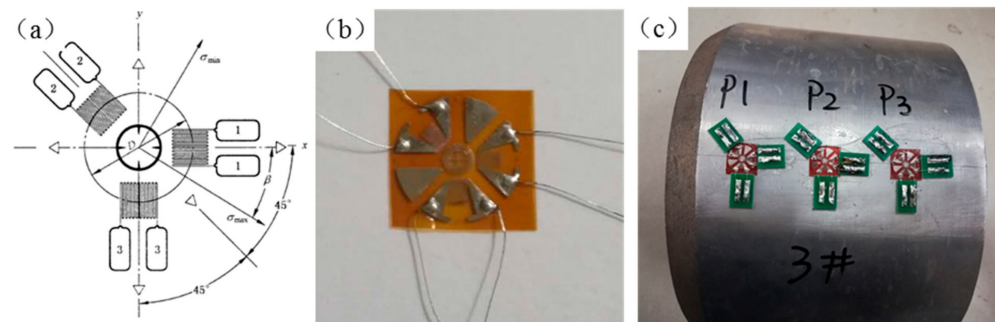


**Figure 4.** Strain gauge rosette type A: (a) Schematic; (b) TJ120-1.5-Ø1.5; and (c) residual stress test.

The tensile samples were cut from the central section of the reduced-scale tapered cylinder along the axial direction and had the following dimensions: Total length, 80 mm; gauge length, 30 mm; width, 8 mm; thickness in the parallel section, 2.5 mm. According to the GB-T228-2002 standard, the tensile tests were performed on a WDW-100A mechanical tensile machine at a tensile rate of 2 mm/min. Three samples were measured to obtain an average for each cold-bulging condition.

Transmission electron microscopy (TEM) (FEI Titan G2 60-300, FEI Company, Hillsboro, OR, USA) was used to characterize the microstructures of the heat-treated tapered cylinder samples. Before TEM analysis, the samples were prepared by grinding and polishing to an 80–90 nm thickness and then punched into flakes of 3 mm in diameter. The disks were further thinned by a twin-jet electro-polishing device (in a solution of 30% nitric acid and 70% methanol at a stable temperature of  $-30\text{ }^{\circ}\text{C}$ ).

### 3. FEM Modeling of Quenching and Cold Bulging Processes

The ABAQUS software was used to perform the FEM simulations of both the solution quenching and subsequent cold bulging processes of the 2A14 aluminum alloy tapered cylinder forgings. This stage had multiple purposes: analyzing the quenching residual stress distribution; studying the evolution of residual stress during the cold bulging process; determining the reduction in quenching residual stress by cold bulging. The quenching and cold bulging processes are complex non-linear thermo-elasto-plastic contact problems, which involve the interactions of the temperature, phase transition, and stress/strain fields. Therefore, a temperature–displacement coupling simulation analysis was required to: (a) calculate the temperature gradient and the residual stress caused by it during quenching, and (b) analyze the stress rebalancing caused by plastic deformation and the residual stress reduction attained by cold bulging. ABAQUS/Standard and ABAQUS/Explicit were used

for the quenching and cold bulging process simulations, respectively. The 2A14 alloy yield strength values required for the simulation model under varying temperature and plastic strain conditions are provided in Figure 5. Table 3 describes the thermal properties (such as thermal conductivity, specific heat capacity, elastic modulus, Poisson's ratio, and thermal expansion coefficient) required for the FEM model [21].

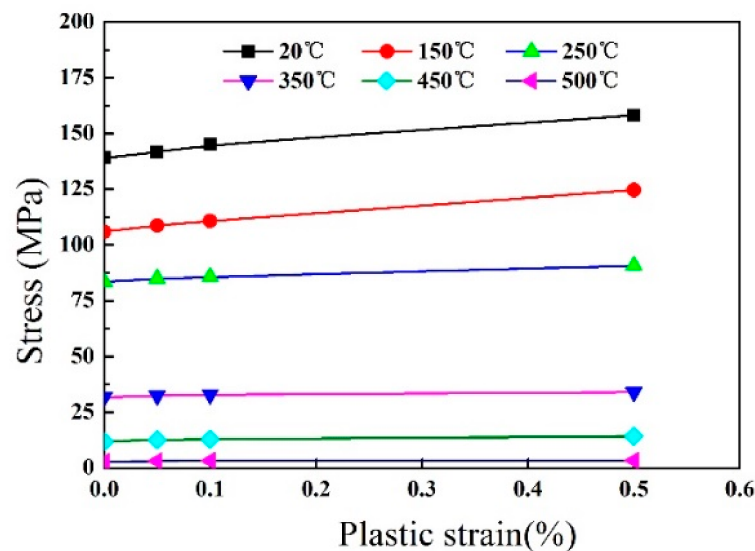


Figure 5. Yield strengths at different temperatures and plastic strains.

Table 3. Thermal properties of 2A14 aluminum alloy.

Temperature /°C	Thermal Conductivity/(W·m <sup>-1</sup> ·K <sup>-1</sup> )	Specific Heat Capacity/(J·kg <sup>-1</sup> ·K <sup>-1</sup> )	Elastic Modulus/GPa	Poisson Ratio	Density/(kg·m <sup>-3</sup> )	Thermal Expansion Coefficient/10 <sup>-6</sup>
20	114.3	809	81.5	0.33	2800	20.8
100	122.3	860	66.2	0.33	2800	21.9
200	130.8	897	49.3	0.33	2800	26.1
300	145.1	922	31.0	0.33	2800	27.0
400	124.5	872	25.3	0.33	2800	26.8
500	122.7	985	–	0.33	2800	27.3

The size of the FEM simulation model was the same as that of the reduced-scale tapered cylinder forging samples used in the experiments (Figure 1). Due to the axisymmetric geometry and boundary conditions of the tapered cylinder forgings, only 1/24 of the sample was used to establish a simplified model for the quenching and cold bulging processes (Figure 6), significantly reducing the simulation calculation time. For the quenching process simulation, 3-dimensional, 8-node linear heat transfer (C3D8T) elements were used. Accordingly, 3-dimensional, 8-node trilinear displacement and temperature, reduced integration, hourglass control (C3D8RT) elements were used for the cold bulging process simulation. The total elements of each simulation model were 9600. The quenching and cold bulging process boundary conditions were consistent with those reported in the experiments discussed above (Figures 2 and 3). The quenching residual stress field was applied as the initial condition in the subsequent cold bulging process simulation, where the effect of the cold bulging ratio on the residual stress reduction performance was also investigated. The cold bulging ratios of 0, 1, 2, 3, and 4% were simulated. The pressure velocity of the bulging die mold was 5 mm/s for all cold bulging simulation scenarios.

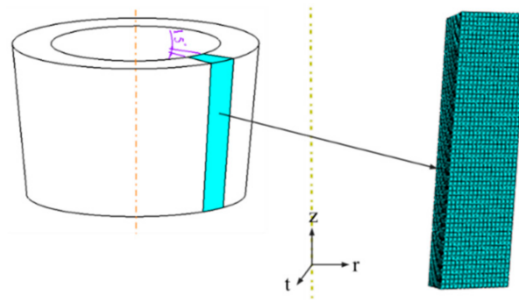


Figure 6. Simplified simulation model and mesh generation.

## 4. Results and Discussion

### 4.1. FEM Simulation Results

The residual stress nephogram at the cross-section of the 2A14 tapered cylinder forging after quenching is displayed Figure 7. As can be observed, the quenching treatment induced a larger residual tensile stress in the central region and a greater residual compressive stress in the exterior region of the tapered cylinder forging, establishing the equilibrium of the stress system. The hoop residual stress ( $\sigma_t$ ) and axial residual stress ( $\sigma_z$ ) levels were much higher than that of the radial residual stress ( $\sigma_r$ ), while the residual stress concentration area in the r-direction was much smaller than those in the t- and z-directions. The hoop tensile residual stress in the center region fluctuated between 120 and 183 MPa, while the tensile axial stress ranged between 115 and 140 MPa. The hoop compression residual stress in the exterior region was between  $-131$  and  $-162$  MPa, while the compressive axial stress was between  $-125$  and  $-149$  MPa.

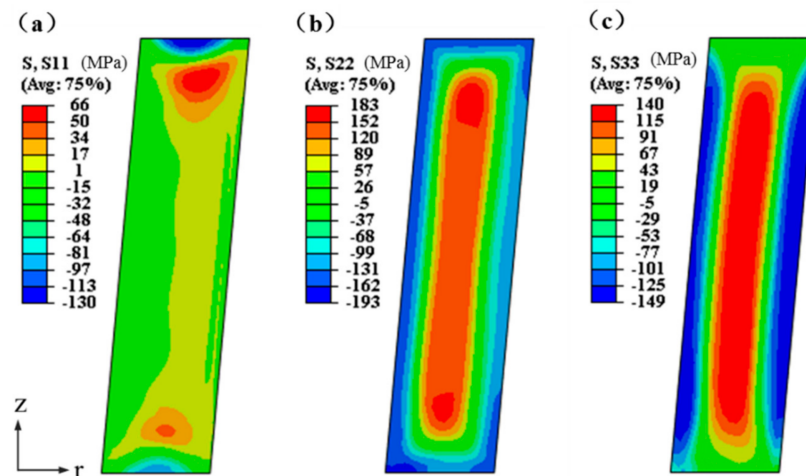
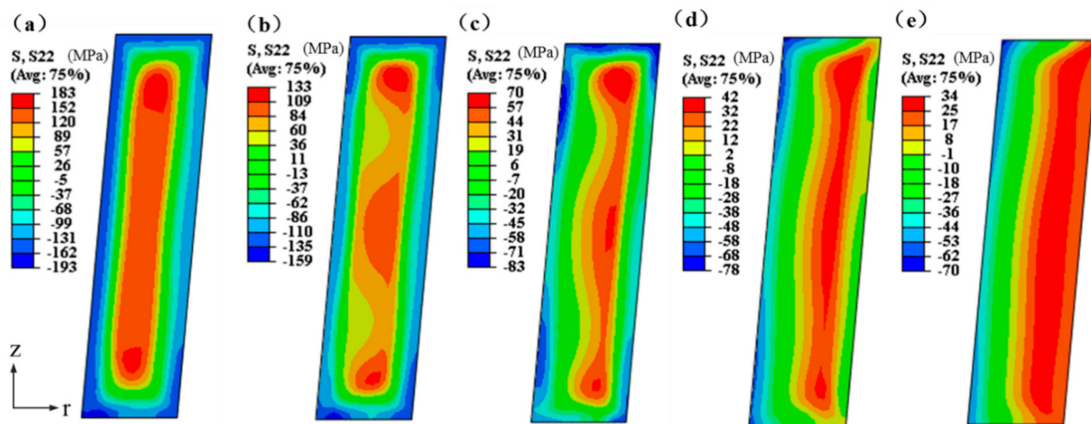


Figure 7. Residual stresses nephogram of the 2A14 tapered cylinder forging in the r-, t-, and z-directions after quenching: (a)  $\sigma_r$ ; (b)  $\sigma_t$ ; and (c)  $\sigma_z$ .

To determine the effect of the cold bulging ratio on the quenching residual stress reduction performance, six cold bulging simulation scenarios with ratios of 0, 1, 2, 3, 3.5, and 4% were investigated in this study. Figures 8 and 9 illustrate the t- and z-direction residual stress nephograms at the cross-section of the 2A14 tapered cylinder forging with different cold bulging ratios. It can be observed that, when the bulging ratio was below 4%, the residual stress levels  $\sigma_t$  and  $\sigma_z$  decreased as the bulging ratio increased. At lower cold bulging ratios ( $\leq 3\%$ ), the hoop and axial stresses both exhibited typical characteristics of tensile stress in the center region and compressive stress in the exterior region of the forging. When the cold bulging ratio exceeded 3%, the hoop residual stress exhibited a large stress gradient along the radial direction. The hoop residual stress on the interior side of the tapered cylinder forging was compressive, whereas on the exterior side it was tensile.

Additionally, the exterior tensile stress exhibited an upward tendency with the increasing cold bulging ratio.



**Figure 8.** Residual stresses nephogram of the 2A14 tapered cylinder forging in the t-direction under different cold bulging ratio conditions: (a) 0%; (b) 1.0%; (c) 2.0%; (d) 3.0%; and (e) 4.0%.

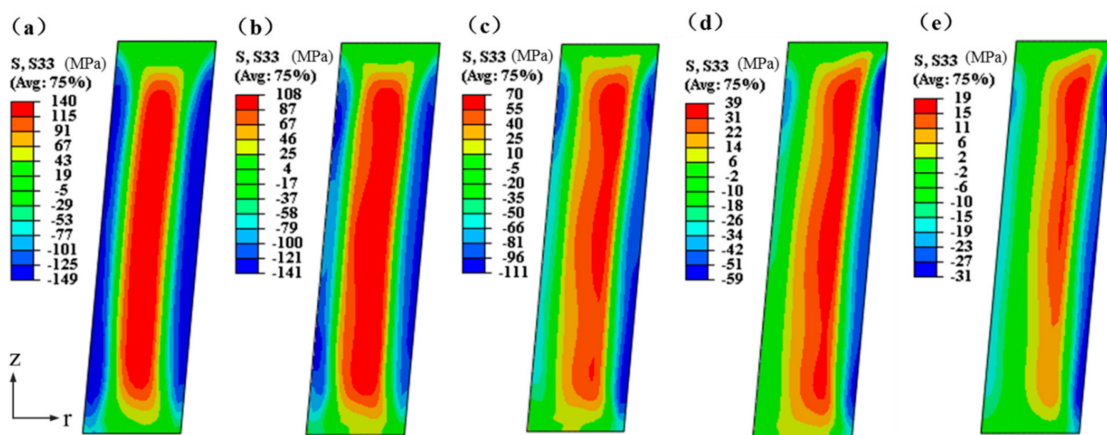


**Figure 9.** Residual stresses nephogram of the 2A14 tapered cylinder forging in the z-direction under different cold bulging ratio conditions: (a) 0%; (b) 1.0%; (c) 2.0%; (d) 3.0%; and (e) 4.0%.

Figure 10 illustrates the residual stresses of the quenched tapered cylinder forgings along path 1 under different cold bulging ratios. As the cold bulging ratio increased, while remaining below 3%, both the hoop and axial residual stresses in the central region of the forgings significantly increased. On the contrary, when the cold bulging ratio exceeded 3%, the reduction rates of both residual stress types became insignificant. Therefore, when considering the optimal cold bulging ratio conditions so as to maximize the reducing effect on the residual tensile stresses in the central region of the forging, the minimum cold bulging ratio was set at 3%. Figure 11 illustrates the residual stresses of the quenched tapered cylinder forging along path 2, under different cold bulging ratios. As the cold bulging ratio increased but remained below 3%, both the hoop and axial residual stresses in the exterior region of the forging sharply decreased. For a cold bulging ratio above 3%, the hoop residual stress on the exterior side of the forging considerably dropped, even transitioning from compressive to tensile stress. Additionally, the tensile stress tended to increase along with the increasing cold bulging ratio. Therefore, in order to maximize the reducing effect on the residual stress in the exterior region, the upper limit of the cold bulging ratio should be less than 3.5%.

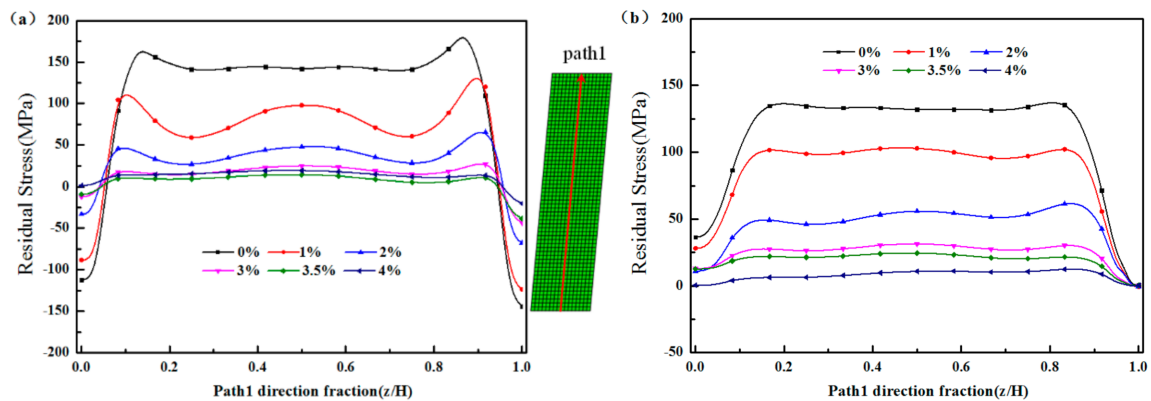


**Figure 10.** Residual stresses of the quenched tapered cylinder forgings along path 1 under different cold bulging ratio conditions: (a)  $\sigma_t$  and (b)  $\sigma_z$ .

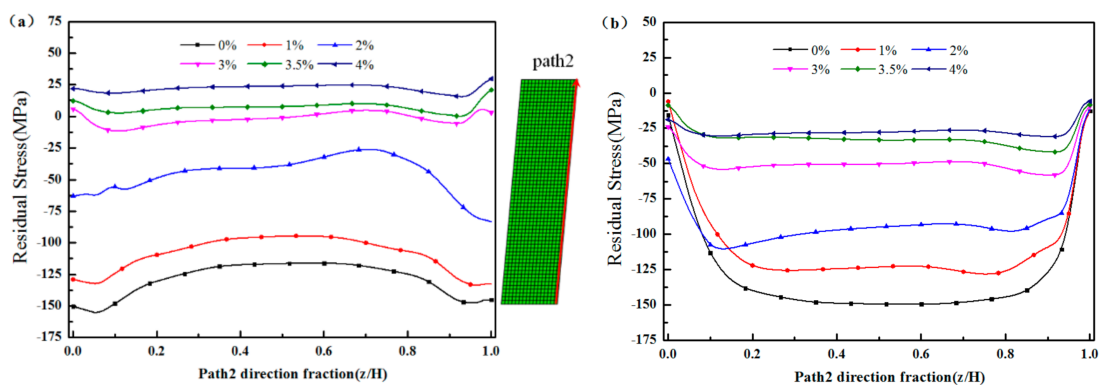


**Figure 11.** Residual stresses of the quenched tapered cylinder forgings along path 2 under different cold bulging ratio conditions: (a)  $\sigma_t$  and (b)  $\sigma_z$ .

#### 4.2. Experimental Results and Discussion

The residual stresses measured by the hole drilling strain-gauge method for all samples are shown in Figure 12, indicating compressive stress at the surface. The results revealed that the residual stress magnitude of sample A, which exhibited natural aging after quenching, was as high as 113–130 MPa—the highest among all samples. Table 4 shows the experimental and simulation results of quenching residual stress of sample A; the test results are in good agreement with the results of the FEM simulation. The residual stress of sample B, which underwent artificial aging after quenching, was 106–120 MPa. Intriguingly, the experimental results showed that, compared with natural aging treatment, artificial aging at 160 °C for 8 h can reduce the quenching residual stress by 7–10 MPa (~7%). However, it was also observed that artificial aging had no significant effect in reducing the residual stress of the 2A14 aluminum alloy tapered cylinder forging samples. Godlewski et al. [22] studied the effects of different aging times and temperatures on the reduction in quenching residual stresses and determined that artificial aging treatment could achieve a 10–35% reduction. It was therefore inferred that artificial aging alone was not sufficient to adequately reduce the quenching residual stress of the samples.

The residual stress values of samples C (2% cold bulging) and D (3% cold bulging) were approximately 19 MPa and 16 MPa, respectively. Their quenching residual stress reduction percentages were compared to that of the sample with natural aging (Figure 13). The results indicated that the quenching residual stress of the cylinder forgings with 2% cold bulging decreased by 95–110 MPa. When the cold bulging rate was increased to 3%, the increase in the reduction percentage was marginal.

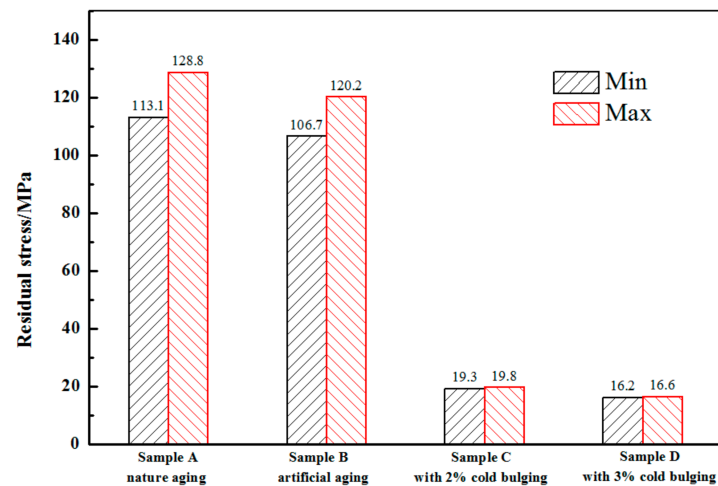


Figure 12. Residual stresses magnitudes as measured via the hole drilling strain-gauge method.

Table 4. Experimental and simulation results of quenching residual stress of taper cylinder forging.

Test Points	Experimental Results					Simulation Results	
	$\sigma_{\max}/\text{MPa}$	$\sigma_{\min}/\text{MPa}$	$\beta/^\circ$	$\sigma_t/\text{MPa}$	$\sigma_z/\text{MPa}$	$\sigma_t/\text{MPa}$	$\sigma_z/\text{MPa}$
P1	−131.8	−103.8	−0.6	−105.9	−129.7	−125.8	−143.3
P2	−125.7	−114.1	−1.2	−122.1	−117.8	−116.4	−149.1
P3	−128.8	−121.4	1.1	−126.9	−123.3	−121.5	−146.2

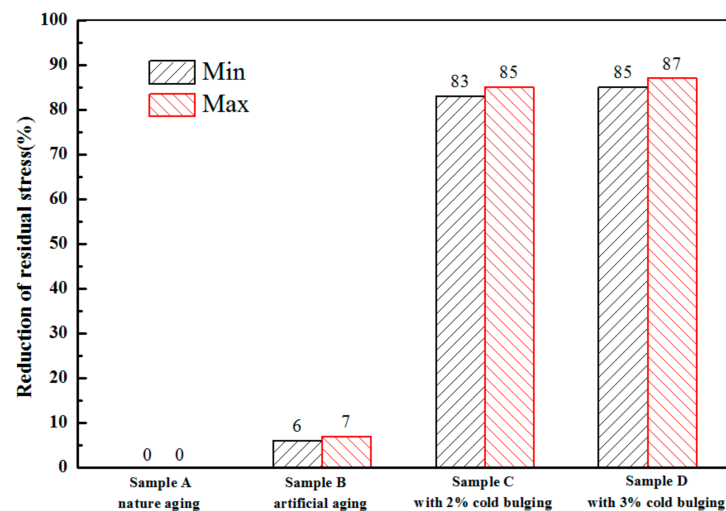


Figure 13. Comparison of residual stress reduction percentage between artificially and naturally aged samples.

When an object sustains non-uniform plastic deformation due to inhomogeneous temperature distribution, quenching residual stress is manifested. Relatively large tensile and compressive stresses can be observed at the core and surface of the quenched forgings, respectively. Residual stress is a stress system that exists in a body without external forces. Assuming a uniform plastic strain acted on the material during the cold deformation process. Cold deformation causes plastic deformation with the opposite sign of the residual stress, thus relieving the material from the residual stress. When the external load is eliminated, the internal stress is rebalanced, and the overall residual stress level of the object is reduced [23]. It was suggested that the quenching residual stress was effectively reduced after the material underwent plastic deformation, but it was not completely

released. As shown in Figure 13, under 2–3% of cold bulging, the quenching residual stress of the tapered cylinder forgings was effectively reduced by approximately 85%, which was in good agreement with the results of the FEM simulation.

Table 5 presents the results of some published works regarding the reduction in residual stresses in aluminum alloys via cold working methods. It can be deduced that our proposed 2–3% cold bulging strategy achieved equally satisfying results, attaining an 83–87% residual stress reduction in the tapered cylinder forgings. However, 2 or 3% cold bulging may not provide the optimal conditions for stress reduction in larger-sized tapered cylinder forgings. Therefore, for tapered cylinder forgings with different materials, quenching conditions, and geometric dimensions, the ideal cold bulging process conditions should be re-optimized.

**Table 5.** The results of residual stress reduction via cold working presented by other researchers.

Alloy	Sample Dimension (mm)	Method of Cold Deformation	Residual Stress Reduction (%)	Reference
7050	5600 × 760 × 121	Cold compression	43–79%	[10]
7050	340 × 127 × 124	Cold compression	more than 90%	[3]
7050	1270 × 406 × 127	Cold stretching	more than 90%	[3]
A357	Ø80 × h160	Cold stretching	81.5–94.9%	[9]
2A14	Ø170 × b30 × h120	Cold bulging	85–87%	Present study

The mechanical properties of the aged samples (i.e., ultimate tensile strength (UTS), yield strength (YS), and elongation percentage) with cold bulging at different ratios are presented in Figure 14. The UTS and YS values increased along with the increasing cold bulging ratio. At room temperature, when the ratio was increased from 0 to 4.0%, these parameters developed as follows: UTS increased from 416 to 481 MPa (15.6% increase); YS increased from 353 to 408 MPa (15.5% increase); elongation increased from 6.3 to 8.0% (26.9% increase). However, with a further increase in the cold bulging ratio the elongation started to decrease. Numerous related studies have confirmed that for the majority of age-hardened aluminum alloys, the introduction of cold deformation before artificial aging can promote precipitation strengthening and improve the mechanical properties of the material. The precipitation phases of the 2A14 aluminum alloy were greatly affected by the relative concentration of solute atoms in the material. The  $C_{Cu}/C_{Mg}$  ratio of the 2A14 aluminum alloy used in this study was  $9.16 > 8$  (Table 1); therefore, the  $\theta$  phase ( $Al_2Cu$ ) and its transition phase were the main strengthening phases, and the aging precipitation sequence was: GP zone  $\rightarrow \theta'' \rightarrow \theta' \rightarrow \theta$  [24]. Figure 15a illustrates the scanning transmission electron microscopy (STEM) micrograph of the aged sample without cold bulging, where multiple intersecting needle-like precipitates with lengths of 50–60 nm were detected. The STEM micrograph of the aged sample with 2% cold bulging (Figure 15b) indicates that, compared to the sample without cold bulging, the corresponding needle-like precipitated phases exhibited smaller sizes, higher density, and a more uniform distribution. In accordance with the selected area electron diffraction (SAED) pattern, the needle-like precipitates were identified as  $\theta'$  fine precipitates. These results further confirmed that cold bulging can effectively promote precipitation during the aging process and thus improve the mechanical properties of the 2A14 forgings.

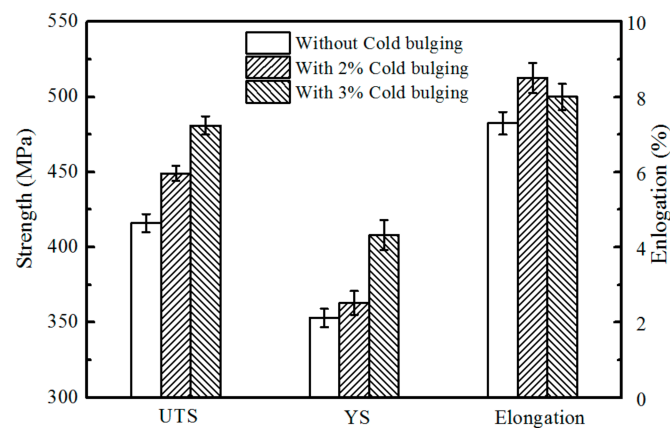


Figure 14. Mechanical properties of the samples under different cold bulging conditions.

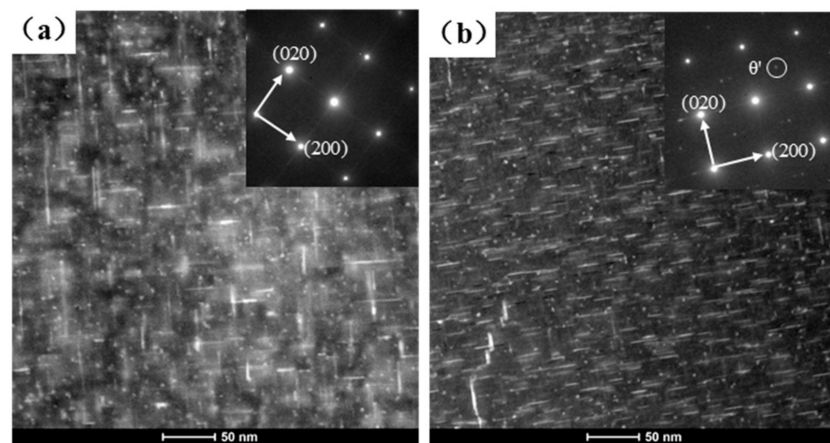


Figure 15.  $\{001\}_{Al}$  TEM images of the as-aged samples with cold bulging at different ratios: (a) Without cold bulging and (b) with 2% cold bulging.

## 5. Conclusions

In the present study, a novel cold bulging process was designed to reduce the quenching residual stresses in 2A14 aluminum alloy tapered cylinder forgings. In this context, its effects on the aging precipitation behavior and mechanical properties of the processed samples were also studied. The following conclusions were drawn:

- (1) Experimental and FEM simulation results demonstrated that 2–3% cold bulging effectively reduced the quenching residual stress of the tapered cylinder forgings by 95–110 MPa. No discernible benefit or disadvantage was reported for cold bulging ratios above 3%.
- (2) Upon increasing the extent of cold bulging, the driving force responsible for the precipitation of the strengthening phase during the aging process was enhanced. As a result, the number, density, and uniformity of the precipitated phases increased, thereby improving the mechanical properties.
- (3) The mechanical properties of the 2A14 aluminum alloy tapered cylinder forgings were further improved with the extension of the cold bulging process. The optimal mechanical properties were achieved when the cold bulging ratio was 3%, with a UTS of 481 MPa, YS of 408 MPa, and elongation of 8.0%.

**Author Contributions:** Conceptualization, B.W. and Y.Y.; software, S.H.; validation, H.H.; formal analysis, H.H.; investigation, B.W.; resources, Y.Y.; data curation, H.H.; writing—original draft preparation, B.W.; writing—review and editing, S.H.; visualization, H.H.; supervision, Y.Y.; funding acquisition, Y.Y. All authors have read and agreed to the published version of the manuscript.

**Funding:** This research was funded by the General Program of Natural Science Foundation of Hunan Province (Grant No. 2020JJ4709) and the Project of Innovation-Driven Plan for PostGraduate in Central South University (No. 2017ZZTS030).

**Data Availability Statement:** Not applicable.

**Conflicts of Interest:** The authors declare no conflict of interest.

## References

1. Zhang, Y.; Yi, Y.; Huang, S.; Dong, F.; Wang, H. Investigation of the quenching sensitivity of forged 2A14 aluminum alloy by time-temperature-tensile properties diagrams. *J. Alloys Compd.* **2017**, *728*, 1239–1247. [\[CrossRef\]](#)
2. Ye, S.; Chen, K.; Liu, L.; Chen, S.; Zhu, C. Prediction and Experimental of Yield Strengths of As-Quenched 7050 Aluminum Alloy Thick Plates after Continuous Quench Cooling. *Metals* **2019**, *10*, 26. [\[CrossRef\]](#)
3. Koç, M.; Culp, J.; Altan, T. Prediction of residual stresses in quenched aluminum blocks and their reduction through cold working processes. *J. Mater. Process. Technol.* **2006**, *174*, 342–354. [\[CrossRef\]](#)
4. Citarella, R.; Carlone, P.; Sepe, R.; Lepore, M.A. DBEM crack propagation in friction stir welded aluminum joints. *Adv. Eng. Softw.* **2016**, *101*, 50–59. [\[CrossRef\]](#)
5. Citarella, R.G.; Cricri, G.; Lepore, M.A.; Perrella, M. Assessment of Crack Growth from a Cold Worked Hole by Coupled FEM-DBEM Approach. *Key Eng. Mater.* **2014**, *557–558*, 669–672. [\[CrossRef\]](#)
6. Araghchi, M.; Mansouri, H.; Vafaei, R. The Effects of Quenching Media and Aging on Residual Stress and Mechanical Properties of 2024 Aluminum Alloy. In Proceedings of the Iran International Aluminum Conference (IIAC2016), Tehran, Iran, 11–12 May 2016.
7. Gur, C.H. Investigation of the influence of specimen geometry on quench behaviour of steels by X-ray determination of surface residual stresses. *Int. J. Mech. Sci.* **2002**, *44*, 1335–1347. [\[CrossRef\]](#)
8. Cui, J.-D.; Yi, Y.-P.; Luo, G.-Y. Numerical and Experimental Research on Cold Compression Deformation Method for Reducing Quenching Residual Stress of 7A85 Aluminum Alloy Thick Block Forging. *Adv. Mater. Sci. Eng.* **2017**, *2017*, 1–6. [\[CrossRef\]](#)
9. Yang, X.; Zhu, J.; Nong, Z.; Lai, Z.; He, N. FEM simulation of quenching process in A357 aluminum alloy cylindrical bars and reduction of quench residual stress through cold stretching process. *Comput. Mater. Sci.* **2013**, *69*, 396–413. [\[CrossRef\]](#)
10. Zhang, Z.; Yang, Y.; Li, L.; Chen, B.; Tian, H. Assessment of residual stress of 7050-T7452 aluminum alloy forging using the contour method. *Mater. Sci. Eng. A* **2015**, *644*, 61–68. [\[CrossRef\]](#)
11. Klamecki, B.E. Residual stress reduction by pulsed magnetic treatment. *J. Mater. Process. Technol.* **2003**, *141*, 385–394. [\[CrossRef\]](#)
12. Lu, A.; Tang, F.; Luo, X.; Mei, J.; Fang, H. Research on residual-stress reduction by strong pulsed magnetic treatment. *J. Mater. Process. Technol.* **1998**, *74*, 259–262. [\[CrossRef\]](#)
13. Cai, Z.; Huang, X. Residual stress reduction by combined treatment of pulsed magnetic field and pulsed current. *Mater. Sci. Eng. A* **2011**, *528*, 6287–6292. [\[CrossRef\]](#)
14. Araghchi, M.; Mansouri, H.; Vafaei, R.; Guo, Y. A novel cryogenic treatment for reduction of residual stresses in 2024 aluminum alloy. *Mater. Sci. Eng. A* **2017**, *689*, 48–52. [\[CrossRef\]](#)
15. Wei, L.; Wang, D.; Li, H.; Xie, D.; Ye, F.; Song, R.; Zheng, G.; Wu, S. Effects of Cryogenic Treatment on the Microstructure and Residual Stress of 7075 Aluminum Alloy. *Metals* **2018**, *8*, 273. [\[CrossRef\]](#)
16. Li, Y.; Liu, Z.; Bai, S.; Zhou, X.; Wang, H.; Zeng, S. Enhanced mechanical properties in an Al-Cu-Mg-Ag alloy by duplex aging. *Mater. Sci. Eng. A* **2011**, *528*, 8060–8064. [\[CrossRef\]](#)
17. Ghosh, S. Influence of Cold Deformation on the Aging Behaviour of Al-Cu-Si-Mg Alloy. *J. Mater. Sci. Technol.* **2011**, *27*, 193–198. [\[CrossRef\]](#)
18. He, H.; Yi, Y.; Huang, S.; Zhang, Y. Effects of cold predeformation on dissolution of second-phase Al<sub>2</sub>Cu particles during solution treatment of 2219 Al-Cu alloy forgings. *Mater. Charact.* **2018**, *135*, 18–24. [\[CrossRef\]](#)
19. Tong, D.; Yi, Y.; He, H.; Huang, S.; Guo, W. Manufacturing large 2A14 aluminium alloy cylinders by a warm rolling technology. *Mater. Sci. Technol.* **2020**, *36*, 1534–1546. [\[CrossRef\]](#)
20. Wang, J.; Lu, Y.; Zhou, D.; Zhou, G.; Xu, W.; Yang, X. Production process of 2A14 aluminum alloy forged ring. *Heat Treat. Met.* **2018**, *43*, 231–235.
21. Zhang, Y.; Yi, Y.; Huang, S.; He, H. Influence of Temperature-Dependent Properties of Aluminum Alloy on Evolution of Plastic Strain and Residual Stress during Quenching Process. *Metals* **2017**, *7*, 228. [\[CrossRef\]](#)
22. Godlewski, L.A.; Su, X.; Pollock, T.M.; Allison, J.E. The Effect of Aging on the Relaxation of Residual Stress in Cast Aluminum. *Met. Mater. Trans. A* **2013**, *44*, 4809–4818. [\[CrossRef\]](#)
23. Robinson, J.; Hossain, S.; Truman, C.; Paradowska, A.; Hughes, D.; Wimpory, R.; Fox, M. Residual stress in 7449 aluminium alloy forgings. *Mater. Sci. Eng. A* **2010**, *527*, 2603–2612. [\[CrossRef\]](#)
24. Lan, J.; Shen, X.; Liu, J.; Hua, L. Strengthening mechanisms of 2A14 aluminum alloy with cold deformation prior to artificial aging. *Mater. Sci. Eng. A* **2019**, *745*, 517–535. [\[CrossRef\]](#)